Role of Adenosine Kinase In Sphingosine-1-Phosphate Receptor 1-Induced Mechano-Hypersensitivities

Filomena Lauro
Saint Louis University School of Medicine
Luigino Antonio Giancotti
Saint Louis University School of Medicine
Grant Kolar
Saint Louis University School of Medicine
Caron Harada
Saint Louis University School of Medicine
Taylor A Harmon
University of Florida
Timothy J Garrett
University of Florida
Daniela Salvemini (daniela.salvemini@health.slu.edu)
Saint Louis University School of Medicine https://orcid.org/0000-0002-0612-4448

Short Report

Keywords: Sphingosine-1-phosphate receptor 1, adenosine receptor subtype 3, adenosine kinase, neuroinflammation, mechano-hypersensitivities.

Posted Date: September 21st, 2021

DOI: https://doi.org/10.21203/rs.3.rs-852148/v1

Version of Record: A version of this preprint was published at Cellular and Molecular Neurobiology on November 13th, 2021. See the published version at https://doi.org/10.1007/s10571-021-01162-8.

Abstract

Emerging evidence implicates the sphingosine-1-phosphate (S1P) receptor subtype 1 (S1PR1) in the development of neuropathic pain. Continued investigation of the signaling pathways downstream of S1PR1 are needed to support development of S1PR1 antagonists. In rodents, intrathecal (i.th.) injection of SEW2871, a selective S1PR1 agonist, activates the nod-like receptor family, pyrin domain containing 3 (NLRP3) inflammasome, increases interleukin-1β (IL-1β) and causes behavioral hypersensitivity. I.th. injection of a IL-1β receptor antagonist blocks SEW2871-induced hypersensitivity, suggesting that IL-1β contributes to S1PR1's actions. Interestingly, previous studies have suggested that IL-1β increases the expression/activity of adenosine kinase (ADK), a key regulator of adenosine signaling at its receptors (ARs). Increased ADK expression reduces adenosine signaling whereas inhibiting ADK restores the action of adenosine. Here, we show that SEW287-induced behavioral hypersensitivity is associated with increased expression of ADK in astrocytes of the dorsal horn of the spinal cord (DH-SC). Moreover, the ADK inhibitor, ABT702, blocks SEW2871-induced hypersensitivity. These findings link ADK activation to S1PR1. If SEW2871-induced pain is mediated by IL-1β, which in turn activates ADK and leads to mechano-allodynia, then blocking ADK should attenuate IL-1β effects. In support of this idea, recombinant rat (rrIL-1β)-induced allodynia was blocked by at least 90% with ABT702, functionally linking ADK to IL-1β. Moreover, the selective A_3AR antagonist, MRS1523, prevents the ability of ABT702 to block SEW2871 and IL-1β-induced allodynia, implicating A_3AR signaling in the beneficial effects exerted by ABT702. Our findings provide novel mechanistic insight into how S1PR1 signaling in the spinal cord produces hypersensitivity through IL1-b and ADK activation.

Introduction

Recent epidemiological studies on chronic pain reveal that 50.0 million of U.S. adults (20.4%) have experienced chronic pain and 19.6 million (8.0%) have experienced high-impact chronic pain (Dahlhamer et al. 2018). Since pain drugs often fail to achieve adequate relief in patients, and opioid treatments are associated with abuse and addiction, developing new pain medicines is crucial. Over the last several years, the sphingosine-1-phosphate (S1P) receptor subtype 1 (S1PR1) has emerged as an attractive molecular target for therapeutic intervention (Squillace et al. 2020). Several studies found that alterations in sphingolipid metabolism in the spinal dorsal horn increase S1P production and contribute to hypersensitivity associated with cancer pain (Grenald et al. 2017), opioid-induced hyperalgesia (Muscoli et al. 2010; Doyle et al. 2020a), neuropathic pain caused by chemotherapy (Stockstill et al. 2019; Janes et al. 2014), multiple sclerosis (Doolen et al. 2018) or traumatic peripheral nerve injury (Chen et al. 2019). Blocking S1PR1 with functional or competitive S1PR1 antagonists prevents and reverses neuropathic pain states of various etiologies (Chen et al. 2019; Squillace et al. 2020). Moreover, studies in breast cancer patients showed that S1PR1 is a potential molecular driver of sensory peripheral neuropathy induced by chemotherapy (Chua et al. 2020). In the spinal cord, S1PR1 activation leads to the development of mechanical and thermal hypersensitivity through nucleotide-binding oligomerization domain-like receptor protein 3 (NLRP3) inflammasome activation and interleukin-1β (IL-1β) signaling

(Doyle et al. 2019). IL-1β, a potent neuroexcitatory, inflammatory and pronociceptive cytokine (Rossi et al. 2014) has been linked to the development of S1PR1-induced hypersensitivity (Doyle et al. 2019), but the mechanisms whereby IL-1β contributes to S1PR1's induced hypersensitivity are not known. Here, we provide evidence that IL-1β drives S1PR1's effects through alterations in the adenosine pathway in the spinal cord that are dependent upon adenosine kinase. Our findings uncover the existence of a functional connection between S1PR1 and adenosine signaling.

Material And Methods

Animals

Female or male Sprague-Dawley rats (200-220 g) were purchased from Envigo Laboratories (Indianapolis, IN USA). Animals of the same sex were housed 3 per cage with 12-hour light/dark cycles and food/water ad libitum. All experiments were conducted in accordance with the National Institutes of Health, the International Association for the Study of Pain guidelines for laboratory animal welfare, and following the Animal Utilization Protocol #2241 approved by the Saint Louis University Institutional Animal Care and Use Committee.

Test Compounds

Fingolimod (FTY720) and SEW2871 were purchased from Cayman Chemical (Ann Arbor, Michigan). Recombinant rat IL-1β (rrIL-1β) was purchased from Bio-Techne (Minneapolis, Minnesota), MRS1523, [3-propyl-6-ethyl-5[(ethylthio)carbonyl]-2-phenyl-4-propyl-3-pyridinecarboxylate] from Sigma (St. Louis, MO, USA), ABT-702 dihydrochloride 5-(3-Bromophenyl)-7-[6-(4-morpholinyl)-3-pyrido[2,3-d]byrimidin-4-amine dihydrochloride was purchased from Tocris. TASP0277308 was synthesized as previously reported (Fujii et al. 2012a).

Drug Delivery

Drugs were co-administrated in a single i.th. injections performed using the Wilcox method (Hylden and Wilcox 1980): rats were lightly anesthetized with isoflurane and a 50 µL Hamilton syringe (Hamilton, Reno, NV USA) with a 25-ga needle was inserted between the L5/L6 vertebrae puncturing the dura (confirmed by presence of reflexive tail flick and hind limbs) and vehicle or test substance(s) (10 µl) was injected. The vehicle used for all i.th. injections of test agents was 3% (for SEW2871, ABT702 and rrIL-1β), or 15 % (for A-438079) DMSO in saline. The vehicle used for all oral administration of test agents was 5% DMSO/0.5% methylcellulose in water (0.2-mL dosing volume). The vehicle used for i.p. injections was 50% DMSO/saline.

Estrus smears

Rat vaginal smears were taken daily for 7 days before and after the experiment to verify normal cyclicity. Cells were placed on a glass slide and analyzed with a light microscope to determine their stage of estrus cycle as described (Byers et al. 2012). All animals displayed a normal 4- to 5-day estrus cycle.

Chronic Constriction Injury (CCI) model of neuropathic pain

CCI to the sciatic nerve of the left hind leg in rats was performed under general anesthesia using the method described by Bennett et al. (Bennett and Xie 1988). Briefly, rats (weighing 200–250 g at the time of surgery) were anesthetized with 3% isoflurane/O_2 inhalation and maintained on 2% isoflurane/O_2 for the duration of surgery. The left thigh was shaved and scrubbed with dermachlor solution (0.2% chlorhexidine gluconate), and a small incision (1–1.5 cm in length) was made in the middle of the lateral aspect of the thigh to expose the sciatic nerve. The nerve was loosely ligated at 3 sites spaced 1 mm apart using 4.0 silk sutures. The surgical site was closed with a skin clip.

Behavioral testing

Mechanical allodynia as a readout was assessed as the hind paw withdrawal response to von Frey hair stimulation using the up-and-down method (Dixon 1980). Briefly, the animals were first acclimatized (30 minutes) in individual clear Plexiglas boxes on an elevated wire mesh platform to facilitate access to the plantar surface of the hind paws. Subsequently, a series of von Frey hairs (1.4, 2, 4, 6, 8, 10, 15, 26 g; Stoelting, Wood Dale, IL USA) were applied perpendicular to the plantar surface of the hind paw, until the filament buckles, for 2–5 s. A test began with the application of the 4 g for rats. A positive response was defined as clear paw withdrawal or shaking. In the event of a positive response, the next lighter hair was applied, whereas the next higher hair was applied in the event of a negative response. At least three readings are obtained after the first positive response and the pattern of response was converted to a 50% paw withdrawal threshold (PWT), using the method described by Chaplan (Chaplan et al. 1994). Mechano-allodynia was defined as a significant (2 SD) decrease in the measured behavior compared to the individual animal's baseline behavior prior to mechanical or pharmacological pain induction.

Western blot analysis

Animals were sacrificed under anesthesia through transcardiac perfusion with cold phosphate-buffered saline (PBS). The dorsal lower lumbar enlargement (L4-L6) of the spinal cord was harvested and flash-frozen in liquid nitrogen. Samples were homogenized, and protein concentrations were determined by bicinchoninic acid (BCA) protein assay (Thermo-Fisher, Waltham, MA). Proteins were denatured in Laemmli buffer and boiled for 5 minutes. Equal amounts of proteins (50 µg or 10 µg) were loaded and resolved by sodium dodecyl sulfate-polyacrylamide gel electrophoresis and transferred to polyvinylidene fluoride membranes. Membranes were blocked for 2 hours at room temperature in 3% bovine serum albumin (BSA) in 1X TBS-T. Anti-NLRP3 (1:1000; Novus Biologicals, Littleton, Colorado, #NBP2-12446), anti-caspase 1 (p20) (1:1000; Santa Cruz Biotechnology, Santa Cruz, California, #sc-398715) and anti-IL-1β antibody (1:1000, Cell Signaling, Danvers, Massachusetts, #12242), anti-adenosine kinase (1:1000; Thermo Fisher Scientific, Waltham, Massachusetts, #PA5-27399) were diluted in 1.5% BSA in 1X TBS-T, and membranes were incubated overnight at 4°C. The bound antibodies were visualized after incubation with peroxidase-conjugated goat anti-rabbit IgG (1:5000, Cell Signaling, #7074) or peroxidase-conjugated bovine anti-mouse IgG secondary antibody (1:5000, Jackson ImmunoResearch, #04-18-15) for 1 hour at

RT. Peroxidase-conjugated antibodies were visualized by enhanced chemiluminescence (Bio-Rad, Hercules, CA). Chemiluminescence antibody signals were documented using Chemidoc XRS+ image system and ImageLab software (BioRad) using exposure settings and quantified for band densitometry. Each membrane was then probed for β-actin (1:5000, Sigma-Aldrich, St. Louis, MO, #A5441) as endogenous loading controls. The antibody used to probe for NLRP3, IL-1β, caspase 1 (p20), adenosine kinase detect the same bands as reported in a previous publications (Doyle et al. 2019; Wahlman et al. 2018). Relative protein expression was quantified by measuring band densitometry. Images for the blots of a protein of interest and their corresponding β-actin were selected for analyses and presentation based on a predetermined upper grayscale value (45000-65000 units) in order to assure linear densitometric values. Images were analyzed using the lane and band functions of the ImageLab™ software. For presentation purposes, the grayscale range was set between 0 units and the predetermined upper grayscale value (45000-65000 units) for the protein of interest and corresponding β-actin prior to exporting as an image file. Post-export modifications of the images were limited to cropping to the regions of interest.

Immunofluorescence

Immunofluorescence was performed using modifications of previously reported methods (Wahlman et al. 2018). After behavioral measurements, rats were perfused with 4%PFA and the lower lumbar enlargement of the spinal cord (L4-L6) was harvested. Tissue was fixed for 30 min with 4% PFA in 1X PBS, washed with PBS and cryoprotected in 30% sucrose before embedding in OCT, and frozen in 2-methylbutane and liquid nitrogen bath. Transverse sections (20 mm) were cut using a cryostat and collected on glass microscope slides. Spinal cord sections were fixed in 4% PFA (10 minutes), blocked (5% donkey serum, 0,5% bovine serum albumin in 1X PBS, for 1 hour), and then immunolabeled using an 18-hour incubation (4°C) with rabbit polyclonal anti-ADK (1:100; Thermo Fisher Scientific, Waltham, Massachusetts, #PA5-27399) and antiglial fibrillary acidic protein (GFAP) (1:1000; Sigma-Aldrich, St. Louis, MO, #G3893). After a series of PBS rinses, sections were incubated for 2 hours with donkey antirabbit Alexa Fluor 594 conjugated (1:250; Jackson ImmunoResearch, #711-585-152) and anti-mouse Alexa Fluor 488 conjugated antibody (1:250; Jackson ImmunoResearch, #715-545-151). The coverslips were mounted with Prolong Gold antifade reagent containing DAPI [4,6-Diamidino-2-phenylindole, dihydrochloride] to label nuclei (Electron Microscopy Sciences, Hatfield, PA). Immunofluorescence images were captured on a Leica TCS SP8 Confocal microscope (Leica Microsystems, Exton, PA) using a 20x lens (0.75 NA) using the same laser power and detector gain for all animals. 8 bit images were collected at 1024x768 resolution and analyzed using the SVI Huygens Object Analysis module (SVI, Netherlands). GFAP and adenosine antibodies were used in a previous publication (Wahlman et al. 2018). GFAP signal in hand selected areas representing lamina 1 and 2 was used to create a ROI for measuring intensity and counting numbers of voxels corresponding to a volume of ADK encompassing the GFAP signal + 1 micrometer of surrounding area in order to approximate astrocytes. One animal from the SEW group was excluded as a clear outlier based on ADK signal out of observed ranges seen for either treatment group. Example images produced using Surface Visualization module of SVI Huygens with the same thresholding applied to both images.

UHPLC-MS/HRMS Analysis for Adenosine and Inosine

All solvents were of LC-MS or better quality. Water with 0.1 % FA and MeOH with 0.1 % FA were purchased from Honeywell Chromasolv™ (Charlotte, NC, USA). Adenosine standard was purchased from ACROS Organics (New Jersey, USA). Inosine standard was purchased from Millipore Sigma (Darmstadt, Germany). Adenosine-$^{13}C_5$ was purchased from Toronto Research Chemicals (Toronto, ON, Canada). Inosine-$^{15}N_4$ was purchased from Cambridge Isotope Laboratories (Tewkesbury, MA, USA).

Combined adenosine and inosine stock solution was prepared in 17:3 H_2O:MeOH + 0.1 % FA at 1 mM from 5 mM individual stocks in same. Calibration standards were prepared in same from 50 nM to 100 µM in half-order of magnitude increments via serial dilution from combined stock (e.g. 50 nM, 100 nM, 500 nM, 1 µM etc.), as were QC standards at 2.5 and 25 µM.

The IS was made at 10 µg/mL in 17:3 H_2O:MeOH + 0.1 % FA from 1 mg/mL individual stocks of adenosine-$^{13}C_5$ and inosine-$^{15}N_4$ in 19:1 H_2O:MeOH + 0.1 % FA.

All samples were injected as extracted by third party (PCA protein precipitation and KOH neutralization), with the addition of IS 3:17 (IS:sample extract).

All analyses were performed on a Dionex UltiMate™ 3000 UHPLC coupled to a Thermo Q Exactive™ Plus Hybrid Quadrupole-Orbitrap™ MS.

Column used was a Phenomenex Kinetex PFP, 1.7 µm, 2.1 x 150 mm. Mobile phase A was 0.1 % FA in H_2O; mobile phase B was 0.1 % FA in MeOH. Isocratic elution at 15 % B was accomplished in 2 min with a 500 µL/min flow rate and a column temperature of 45 °C. Injection volume was 2 µL.

Negative Heated ESI (HESI) parameters were as follows: -3.0 kV spray voltage, 40 % S-lens, 50 au sheath gas, 15 au auxiliary gas, 1 au sweep gas, 350 °C capillary temperature & 275 °C HESI probe temperature.

LC-MS/MS assay for nucleotides

The assay covered the analysis of NAM, NMN, 1-methyl NAM, NAD, NADPH, ATP, GTP, CTP, TTP, UTP, IMP, AMP, CMP, GMP, UMP, and TMP. Detailed protocols for LC-MS/MS assays of oxidized nucleotides were described elsewhere (Petucci et al. 2019).

An aliquot of biological fluid, cell homogenate, or tissue homogenate was quenched with equal volume of 1M PCA and spiked with a mixture of heavy isotope-labeled, nucleotide internal standards followed by the addition of 1M ammonium formate. Samples were vortexed and centrifuged at 18,000 x g for 5 min at 10 °C. and then filtered through an AcroPrep Advance 3K Omega Filter Plate (Pall Corporation) by centrifugation at 3500 x g for 60 min prior to LC-MS/MS analysis. Metabolites were separated on a 2.1 x 50 mm, 3 µm Thermo Scientific Hypercarb column (T = 30°C) using a Dionex Ultimate 3000 UHPLC. The step gradient was 98% A (10 mM ammonium acetate, pH 9.5) and 2% B (ACN) to 64 % A and 36% B over

6.3 min. The step gradient began at 2% B (0.6 ml min-1 flow rate) from 0-0.45 min, was increased from 2% to 36% B (0.6 ml min-1 flow rate) from 0.45-6.3 min, was increased from 36% to 95% B (0.8 ml min-1 flow rate) from 6.3-6.4 min, and was held until 8.4 min. Re-equilibration was performed at 2% B from 8.4-8.5 min (0.7 ml min-1 flow rate) and was held until 11.5 min. The flow returned to 0.6 ml min-1 at 11.6 min and was held until 11.7 min. Quantitation of pyridine nucleotides was achieved using single reaction monitoring (SRM) on a Thermo Scientific Quantiva triple quadrupole mass spectrometer (Thermo Scientific). The mass spectrometer was operated in positive ion mode using electrospray ionization with an ESI capillary voltage of 3500 V. The ion transfer tube temperature was 350 °C and vaporizer temperature was 350°C. The ESI source sheath gas was set to 40, the auxiliary gas was set to 10, and the sweep gas was set to 1. The mass spectrometer was operated with a mass resolution of 0.7 Da, a cycle time of 0.3 s, and nitrogen collision gas of 1.5 mTorr for the generation and detection of product ions of each nucleotide. Collision energies to produce product ions ranged from 16-46 V with RF lens values ranging from 43-85 V.

S1PR1 functional assay

To evaluate the MRS1523 activity on S1PR1, S1PR1 Lysophospholipid (S1P) GPCR cell-based antagonist β-Arrestin assay (The PathHunter® β-Arrestin assay; Eurofins Discovery, Fremont, CA) was performed following the manufacturer's instructions. β-Arrestin recruitment was measured in cells expressing S1PR1. Data was normalized to the maximal and minimal response observed in the presence of EC80 ligand and vehicle. The following EC80 concentrations were used: mEDG1 Arrestin: 0.065μM S1P **(Fig. 2e)**. Percentage inhibition was calculated using the following formula: % Inhibition =100% x (1 - (mean RLU of test sample - mean RLU of vehicle control) / (mean RLU of EC80 control - mean RLU of vehicle control)).Compound activity was analyzed using CBIS data analysis suite (ChemInnovation, CA).

Statistical Analysis

Data are expressed as mean ± SD. No differences were observed between male and female rats behavior ($p < 0.05$) and therefore, where indicated, data were expressed as a single group. Justification for animal numbers was consistent with NIH policy (NOT-OD-15-102), and experiments were randomized to blinded treatment groups, giving 80% power to detect a treatment effect size of 20% compared to a baseline response of 5% at a significance level of 0.05 (Andrews et al. 2016). Behavioral data were analyzed by student's t test, one-way, two-way, or repeated measures ANOVA with Dunnett's or Tukey's pair-wise comparisons. Protein expression data was determined by two-tailed, one-way ANOVA with Tukey's comparisons. All statistical analyses were performed using GraphPad Prism version 9.0 (Graph Pad Inc., San Diego, CA).

Results And Discussion

Intrathecal (i.th.) injection of the highly selective S1PR1 agonist, SEW2871 (2 nmol (Sanna et al. 2004) activates NLRP3 in the dorsal horn of the spinal cord (DH-SC) and evokes significant mechano-allodynia

that is maximal within 2 hours post-injection in both female and male rats (Fig. 1a). NLRP3 is one of seven known nod-like receptors that form multimolecular inflammasome complexes (Kim et al. 2016; Davis et al. 2011) in the CNS that function as intracellular sensors for infectious agents, as well as for host-derived danger signals (Voet et al. 2019; Tsuchiya and Hara 2014; Walsh et al. 2014). On activation, NLRP3 forms the inflammasome complex by binding and stimulating the autoactivation of the cysteine protease caspase-1 that catalyzes the cleavage of proIL-1β to the active form, IL-1β (Lopez-Castejon and Brough 2011; Franchi et al. 2009). At time of peak allodynia (Fig. 1a) and when compared with animals that received its vehicle, SEW2871 causes a significant increase in the expression of the NLRP3 subunit (Fig. 1b), cleaves caspase-1 (Fig. 1c) and increases IL-1β expression (Fig. 1d). IL-1β, a potent neuroexcitatory cytokine (Viviani et al. 2003) released from neurons, microglia and astrocytes (Ren and Torres 2009) contributes directly to S1PR1's induced hypersensitivity (Doyle et al. 2019). Although the molecular mechanisms remain unexplored, we implicate roles for adenosine kinase (ADK), the key determinant of adenosine signaling (Boison 2013; Aronica et al. 2013). In the adult CNS, ADK is highly expressed in astrocytes and is upregulated in response to increased astrocyte reactivity (Boison et al. 2010). Noteworthy, S1PR1 is highly expressed on astrocytes (Healy and Antel 2016; Van Doorn et al. 2010). Astrocytes are a key cellular hub for the pharmacological actions of S1PR1 activity (Chen et al. 2019) and S1PR1 antagonism (Doyle et al. 2020a).

In vitro studies in astrocytes suggested that IL-1β increases the expression/activity of ADK (Aronica et al. 2011). It is well-documented that adenosine signaling is significantly reduced when ADK expression is increased (Boison 2013). We recently reported that activation of the A_3AR subtype, one of adenosine's four known receptors, inhibits behavioral hypersensitivities that accompany many pain states (Jacobson et al. 2020). Moreover, increased expression of ADK in the spinal cord has been linked to decreased adenosine-A_3AR signaling and inhibiting ADK activity blocks the development of hypersensitivity in an A_3AR-dependent manner (Little et al. 2015; Wahlman et al. 2018). Whether S1PR1-induced hypersensitivity is driven by IL-1β and effects downstream of ADK is not known.

Our immunofluorescence data show that the S1PR1 agonist, SEW2871, increases ADK expression in the dorsal horn lamina I and II of the DH-SC (Fig. 1g-i). This increase was associated with astrocytes identified by colocalization staining with the specific astrocyte marker, GFAP (Fig. 1h-i). We measured levels of adenosine and upstream metabolites (ATP, ADP, AMP) or breakdown products (inosine, AMP) using an LC-MS/HRMS assay in DH-SC in response to S1PR1 activation and found no changes **(Suppl. Figure 1–3; Suppl. Table 1).** The LC-HRMS/MS method developed was linear over the measured concentration range of 50 nM to 100 μM and we detected adenosine and inosine in each sample. It is possible that the enzymatic processes were not fully quenched, thus preventing any observation of changes in the tissue samples since these analytes are involved in rapid breakdown processes. In a separate assay, we also measured NAM, NMN, 1-methyl NAM, NAD, NADPH, ATP, GTP, CTP, TTP, UTP, IMP, AMP, CMP, GMP, UMP and TMP. Again, we found no significant differences (data not shown). However, S1PR1-induced ADK expression must have compromised endogenous adenosine signaling, since i.th. injection of the potent (IC_{50} = 1.7 nM) and highly selective non-nucleoside ADK inhibitor, ABT-702 (30

nmol) (Kowaluk et al. 2000) blocked SEW2871-induced hypersensitivity in both female and male rats (Fig. 1a). These findings establish a functional link of ADK activation to S1PR1. Moreover, the anti-allodynic effects of ABT-702 were significantly attenuated in both female and male rats in the presence of MRS1523 (3 nmol), a potent and selective A_3AR antagonist (Little et al. 2015) **(Fig.s 1a, 1f)**, consistent with adenosine signaling at the A_3AR.

If SEW2871-induced pain is mediated by IL-1β, which in turn increases ADK expression/activation and leads to mechano-allodynia, then IL-1β should recapitulate the effects seen with SEW2817. In support of this idea, i.th. injection of recombinant rat IL-1β (rrIL-1β) increases ADK expression in the DH-SC (Fig. 1e) and mechano-allodynia (Fig. 1f). These effects are blocked with ABT702 by at least 90% (Fig. 1f) and MRS1523 attenuates ABT702's ability to block IL-1β-induced allodynia (Fig. 1f), implicating A_3AR signaling in the beneficial effects exerted by ABT702.

Collectively, these results suggest a model whereby S1PR1 activation engages NLRP3, leading to IL-1β formation, increased ADK expression/activation and reduced A_3AR signalling. Blocking ADK engages A_3AR signalling and prevents the development of S1PR1-evoked hypersensitivity. Our findings, which provide novel mechanistic insights into molecular signaling pathways engaged by S1PR1 in the spinal cord, in turn suggest that the beneficial effects of S1PR1 antagonists observed in neuropathic pain (Squillace et al. 2020) may include their ability to restore A_3AR signaling.

We tested this possibility in a well-characterized rat model of traumatic nerve-injury neuropathic pain caused by chronic constriction of the sciatic nerve (CCI) (Bennett and Xie 1988). Two S1PR1 antagonists were used: the competitive S1PR1 antagonist, TASP0277308 (Fujii et al. 2012b) and FTY720, a functional S1PR1 antagonist (Brinkmann et al. 2010; Bigaud et al. 2014). We previously reported that in this model, ADK expression/activation increases in response to nerve injury in the DH-SC at the time of peak allodynia, and that systemic administration of an ADK inhibitor (ABT-70) reverses mechano-allodynia (Little et al. 2015). Moreover, i.th. injection of MRS1523 blocks the effects of ABT-702, consistent with adenosine signaling at the A_3AR. Chronic constriction of the sciatic nerve leads to the development of mechano-allodynia, which peaks around 7 days (Chen et al. 2019). At time of peak mechano-allodynia (7 days after nerve injury), oral administration of TASP0277308 or FTY720 reverses mechano-allodynia in a time-dependent manner (Fig. 2a-b). These effects are abrogated by an i.p. injection of MRS1523 (Fig. 2b). In contrast, the anti-allodynic effects of morphine are not altered by MRS1523 (Fig. 2c), supporting previous findings (Doyle et al. 2020b). TASP0277308 or FTY720 were used at doses (3 mg/kg) used in previous studies (Chen et al. 2019). Moreover, we show that the beneficial effects observed with systemic administration of FTY720 are blocked by i.th. injection of MRS1523, implicating the DH-SC as a prominent site of action (Fig. 2d). In order to exclude any potential effects of MRS1523 as an S1PR1 antagonist, we performed a GPCR cell-based antagonist β-arrestin assay at Eurofins Discovery. MRS1523 did not inhibit S1PR1 agonist activity, confirming that it is not a S1PR1 antagonist (Fig. 2e).

In summary, we present the first evidence that S1PR1-induced behavioral hypersensitivity is mediated by an IL-1β-ADK-A_3AR signaling pathway, bridging the gap in our understanding of the mode of action of S1PR1 antagonists.

Declarations

Acknowledgements

The authors thank Dr. Zhoumou Chen (Saint Louis University, St. Louis, Missouri, USA) for his technical support during the experiments and Dr. Joel Eissenberg (Saint Louis University, St. Louis, Missouri, USA) for editing the manuscript.

Funding This research was supported by Saint Louis University Start Up Fund (DS), NIH/NIDA grant R01DA043543 (DS) and Training Grant T32GM008306-28 (CMH).

Conflicts of interest/Competing interests

DS has patents submitted by Saint Louis University that cover some of the intellectual property described in this manuscript (U.S. patent number 8,747,844 and its divisional, U.S. patent number 8,945,549). All other authors declare no competing financial interests.

Authors' contributions

Ethics approval All animal experiments were conducted in accordance with the National Institutes of Health, the International Association for the Study of Pain guidelines for laboratory animal welfare, and the Saint Louis University Institutional Animal Care and Use Committee.

Part of this data was presented at the poster session of the “Society for Neuroscience” annual meeting (Chicago, 2019).

References

1. Andrews NA, Latremoliere A, Basbaum AI, Mogil JS, Porreca F, Rice ASC, Woolf CJ, Currie GL, Dworkin RH, Eisenach JC, Evans S, Gewandter JS, Gover TD, Handwerker H, Huang W, Iyengar S, Jensen MP, Kennedy JD, Lee N, Levine J, Lidster K, Machin I, McDermott MP, McMahon SB, Price TJ, Ross SE, Scherrer G, Seal RP, Sena ES, Silva E, Stone L, Svensson CI, Turk DC, Whiteside G (2016) Ensuring transparency and minimization of methodologic bias in preclinical pain research: PPRECISE considerations. Pain 157(4):901–909. doi:10.1097/j.pain.0000000000000458
2. Aronica E, Sandau US, Iyer A, Boison D (2013) Glial adenosine kinase–a neuropathological marker of the epileptic brain. Neurochem Int 63(7):688–695. doi:10.1016/j.neuint.2013.01.028

3. Aronica E, Zurolo E, Iyer A, de Groot M, Anink J, Carbonell C, van Vliet EA, Baayen JC, Boison D, Gorter JA (2011) Upregulation of adenosine kinase in astrocytes in experimental and human temporal lobe epilepsy. Epilepsia 52(9):1645–1655. doi:10.1111/j.1528-1167.2011.03115.x
4. Bennett GJ, Xie YK (1988) A peripheral mononeuropathy in rat that produces disorders of pain sensation like those seen in man. Pain 33(1):87–107
5. Bigaud M, Guerini D, Billich A, Bassilana F, Brinkmann V (2014) Second generation S1P pathway modulators: research strategies and clinical developments. Biochim Biophys Acta 1841(5):745–758. doi:10.1016/j.bbalip.2013.11.001
6. Boison D (2013) Adenosine kinase: exploitation for therapeutic gain. Pharmacol Rev 65(3):906–943. doi:10.1124/pr.112.006361
7. Boison D, Chen JF, Fredholm BB (2010) Adenosine signaling and function in glial cells. Cell Death Differ 17(7):1071–1082. doi:10.1038/cdd.2009.131
8. Brinkmann V, Billich A, Baumruker T, Heining P, Schmouder R, Francis G, Aradhye S, Burtin P (2010) Fingolimod (FTY720): discovery and development of an oral drug to treat multiple sclerosis. Nat Rev Drug Discov 9(11):883–897. doi:10.1038/nrd3248
9. Byers SL, Wiles MV, Dunn SL, Taft RA (2012) Mouse estrous cycle identification tool and images. PLoS One 7(4):e35538. doi:10.1371/journal.pone.0035538
10. Chaplan SR, Bach FW, Pogrel JW, Chung JM, Yaksh TL (1994) Quantitative assessment of tactile allodynia in the rat paw. J Neurosci Methods 53(1):55–63
11. Chen Z, Doyle TM, Luongo L, Largent-Milnes TM, Giancotti LA, Kolar G, Squillace S, Boccella S, Walker JK, Pendleton A, Spiegel S, Neumann WL, Vanderah TW, Salvemini D (2019) Sphingosine-1-phosphate receptor 1 activation in astrocytes contributes to neuropathic pain. Proc Natl Acad Sci U S A. doi:10.1073/pnas.1820466116
12. Chua KC, Xiong C, Ho C, Mushiroda T, Jiang C, Mulkey F, Lai D, Schneider BP, Rashkin SR, Witte JS, Friedman PN, Ratain MJ, McLeod HL, Rugo HS, Shulman LN, Kubo M, Owzar K, Kroetz DL (2020) Genomewide Meta-Analysis Validates a Role for S1PR1 in Microtubule Targeting Agent-Induced Sensory Peripheral Neuropathy. Clin Pharmacol Ther 108(3):625–634. doi:10.1002/cpt.1958
13. Dahlhamer J, Lucas J, Zelaya C, Nahin R, Mackey S, DeBar L, Kerns R, Von Korff M, Porter L, Helmick C (2018) Prevalence of Chronic Pain and High-Impact Chronic Pain Among Adults - United States, 2016. MMWR Morb Mortal Wkly Rep 67(36):1001–1006. doi:10.15585/mmwr.mm6736a2
14. Davis BK, Wen H, Ting JP (2011) The inflammasome NLRs in immunity, inflammation, and associated diseases. Annu Rev Immunol 29:707–735. doi:10.1146/annurev-immunol-031210-101405
15. Dixon WJ (1980) Efficient analysis of experimental observations. Annu Rev Pharmacol Toxicol 20:441–462. doi:10.1146/annurev.pa.20.040180.002301
16. Doolen S, Iannitti T, Donahue RR, Shaw BC, Grachen CM, Taylor BK (2018) Fingolimod reduces neuropathic pain behaviors in a mouse model of multiple sclerosis by a sphingosine-1 phosphate

receptor 1-dependent inhibition of central sensitization in the dorsal horn. Pain 159(2):224–238. doi:10.1097/j.pain.0000000000001106

17. Doyle TM, Chen Z, Durante M, Salvemini D (2019) Activation of Sphingosine-1-Phosphate Receptor 1 in the Spinal Cord Produces Mechanohypersensitivity Through the Activation of Inflammasome and IL-1beta Pathway. J Pain 20(8):956–964. doi:10.1016/j.jpain.2019.02.007
18. Doyle TM, Janes K, Chen Z, Grace PM, Esposito E, Cuzzocrea S, Largent-Milnes TM, Neumann WL, Watkins LR, Spiegel S, Vanderah TW, Salvemini D (2020a) Activation of sphingosine-1-phosphate receptor subtype 1 in the central nervous system contributes to morphine-induced hyperalgesia and antinociceptive tolerance in rodents. Pain. doi:10.1097/j.pain.0000000000001888
19. Doyle TM, Largent-Milnes TM, Chen Z, Staikopoulos V, Esposito E, Dalgarno R, Fan C, Tosh DK, Cuzzocrea S, Jacobson KA, Trang T, Hutchinson MR, Bennett GJ, Vanderah TW, Salvemini D (2020b) Chronic Morphine-Induced Changes in Signaling at the A3 Adenosine Receptor Contribute to Morphine-Induced Hyperalgesia, Tolerance, and Withdrawal. J Pharmacol Exp Ther 374(2):331–341. doi:10.1124/jpet.120.000004
20. Franchi L, Eigenbrod T, Munoz-Planillo R, Nunez G (2009) The inflammasome: a caspase-1-activation platform that regulates immune responses and disease pathogenesis. Nat Immunol 10(3):241–247. doi:10.1038/ni.1703
21. Fujii Y, Hirayama T, Ohtake H, Ono N, Inoue T, Sakurai T, Takayama T, Matsumoto K, Tsukahara N, Hidano S, Harima N, Nakazawa K, Igarashi Y, Goitsuka R (2012a) Amelioration of collagen-induced arthritis by a novel S1P1 antagonist with immunomodulatory activities. J Immunol 188(1):206–215. doi:10.4049/jimmunol.1101537
22. Fujii Y, Ueda Y, Ohtake H, Ono N, Takayama T, Nakazawa K, Igarashi Y, Goitsuka R (2012b) Blocking S1P interaction with S1P(1) receptor by a novel competitive S1P(1)-selective antagonist inhibits angiogenesis. Biochem Biophys Res Commun 419(4):754–760. doi:10.1016/j.bbrc.2012.02.096
23. Grenald SA, Doyle TM, Zhang H, Slosky LM, Chen Z, Largent-Milnes TM, Spiegel S, Vanderah TW, Salvemini D (2017) Targeting the S1P/S1PR1 axis mitigates cancer-induced bone pain and neuroinflammation. Pain 158(9):1733–1742. doi:10.1097/j.pain.0000000000000965
24. Healy LM, Antel JP (2016) Sphingosine-1-Phosphate Receptors in the Central Nervous and Immune Systems. Curr Drug Targets 17(16):1841–1850. doi:10.2174/1389450116666151001112710
25. Hylden JL, Wilcox GL (1980) Intrathecal morphine in mice: a new technique. Eur J Pharmacol 67(2–3):313–316. doi:10.1016/0014-2999(80)90515-4
26. Jacobson KA, Giancotti LA, Lauro F, Mufti F, Salvemini D (2020) Treatment of chronic neuropathic pain: purine receptor modulation. Pain. doi:10.1097/j.pain.0000000000001857
27. Janes K, Little JW, Li C, Bryant L, Chen C, Chen Z, Kamocki K, Doyle T, Snider A, Esposito E, Cuzzocrea S, Bieberich E, Obeid L, Petrache I, Nicol G, Neumann WL, Salvemini D (2014) The development and maintenance of paclitaxel-induced neuropathic pain require activation of the sphingosine 1-phosphate receptor subtype 1. J Biol Chem 289(30):21082–21097. doi:10.1074/jbc.M114.569574

28. Kim YK, Shin JS, Nahm MH (2016) NOD-Like Receptors in Infection, Immunity, and Diseases. Yonsei Med J 57(1):5–14. doi:10.3349/ymj.2016.57.1.5
29. Kowaluk EA, Mikusa J, Wismer CT, Zhu CZ, Schweitzer E, Lynch JJ, Lee CH, Jiang M, Bhagwat SS, Gomtsyan A, McKie J, Cox BF, Polakowski J, Reinhart G, Williams M, Jarvis MF (2000) ABT-702 (4-amino-5-(3-bromophenyl)-7-(6-morpholino-pyridin- 3-yl)pyrido[2,3-d]pyrimidine), a novel orally effective adenosine kinase inhibitor with analgesic and anti-inflammatory properties. II. In vivo characterization in the rat. J Pharmacol Exp Ther 295(3):1165–1174
30. Little JW, Ford A, Symons-Liguori AM, Chen Z, Janes K, Doyle T, Xie J, Luongo L, Tosh DK, Maione S, Bannister K, Dickenson AH, Vanderah TW, Porreca F, Jacobson KA, Salvemini D (2015) Endogenous adenosine A3 receptor activation selectively alleviates persistent pain states. Brain 138(Pt 1):28–35. doi:10.1093/brain/awu330
31. Lopez-Castejon G, Brough D (2011) Understanding the mechanism of IL-1beta secretion. Cytokine Growth Factor Rev 22(4):189–195. doi:10.1016/j.cytogfr.2011.10.001
32. Muscoli C, Doyle T, Dagostino C, Bryant L, Chen Z, Watkins LR, Ryerse J, Bieberich E, Neumman W, Salvemini D (2010) Counter-regulation of opioid analgesia by glial-derived bioactive sphingolipids. J Neurosci 30(46):15400–15408. doi:10.1523/JNEUROSCI.2391-10.2010
33. Petucci C, Culver JA, Kapoor N, Sessions EH, Divlianska D, Gardell SJ (2019) Measurement of Pyridine Nucleotides in Biological Samples Using LC-MS/MS. In: Bhattacharya SK (ed) Metabolomics, Methods and Protocols. Springer Science + Business Media, LLC, pp 61–73. doi:https://doi.org/10.1007/978-1-4939-9488-5
34. Ren K, Torres R (2009) Role of interleukin-1beta during pain and inflammation. Brain Res Rev 60(1):57–64. doi:10.1016/j.brainresrev.2008.12.020
35. Rossi S, Motta C, Studer V, Macchiarulo G, Volpe E, Barbieri F, Ruocco G, Buttari F, Finardi A, Mancino R, Weiss S, Battistini L, Martino G, Furlan R, Drulovic J, Centonze D (2014) Interleukin-1beta causes excitotoxic neurodegeneration and multiple sclerosis disease progression by activating the apoptotic protein p53. Mol Neurodegener 9:56. doi:10.1186/1750-1326-9-56
36. Sanna MG, Liao J, Jo E, Alfonso C, Ahn MY, Peterson MS, Webb B, Lefebvre S, Chun J, Gray N, Rosen H (2004) Sphingosine 1-phosphate (S1P) receptor subtypes S1P1 and S1P3, respectively, regulate lymphocyte recirculation and heart rate. J Biol Chem 279(14):13839–13848. doi:10.1074/jbc.M311743200
37. Squillace S, Spiegel S, Salvemini D (2020) Targeting the Sphingosine-1-Phosphate Axis for Developing Non-narcotic Pain Therapeutics. Trends Pharmacol Sci 41(11):851–867. doi:10.1016/j.tips.2020.09.006
38. Stockstill K, Wahlman C, Braden K, Chen Z, Yosten GL, Tosh DK, Jacobson KA, Doyle TM, Samson WK, Salvemini D (2019) Sexually dimorphic therapeutic response in bortezomib-induced neuropathic pain reveals altered pain physiology in female rodents. Pain. doi:10.1097/j.pain.0000000000001697
39. Tsuchiya K, Hara H (2014) The inflammasome and its regulation. Crit Rev Immunol 34(1):41–80. doi:10.1615/critrevimmunol.2013008686

40. Van Doorn R, Van Horssen J, Verzijl D, Witte M, Ronken E, Van Het Hof B, Lakeman K, Dijkstra CD, Van Der Valk P, Reijerkerk A, Alewijnse AE, Peters SL, De Vries HE (2010) Sphingosine 1-phosphate receptor 1 and 3 are upregulated in multiple sclerosis lesions. Glia 58(12):1465–1476. doi:10.1002/glia.21021
41. Viviani B, Bartesaghi S, Gardoni F, Vezzani A, Behrens MM, Bartfai T, Binaglia M, Corsini E, Di Luca M, Galli CL, Marinovich M (2003) Interleukin-1beta enhances NMDA receptor-mediated intracellular calcium increase through activation of the Src family of kinases. J Neurosci 23(25):8692–8700
42. Voet S, Srinivasan S, Lamkanfi M, van Loo G (2019) Inflammasomes in neuroinflammatory and neurodegenerative diseases. EMBO Mol Med 11 (6). doi:10.15252/emmm.201810248
43. Wahlman C, Doyle TM, Little JW, Luongo L, Janes K, Chen Z, Esposito E, Tosh DK, Cuzzocrea S, Jacobson KA, Salvemini D (2018) Chemotherapy-induced pain is promoted by enhanced spinal adenosine kinase levels through astrocyte-dependent mechanisms. Pain 159(6):1025–1034. doi:10.1097/j.pain.0000000000001177
44. Walsh JG, Muruve DA, Power C (2014) Inflammasomes in the CNS. Nat Rev Neurosci 15(2):84–97. doi:10.1038/nrn3638

Figures

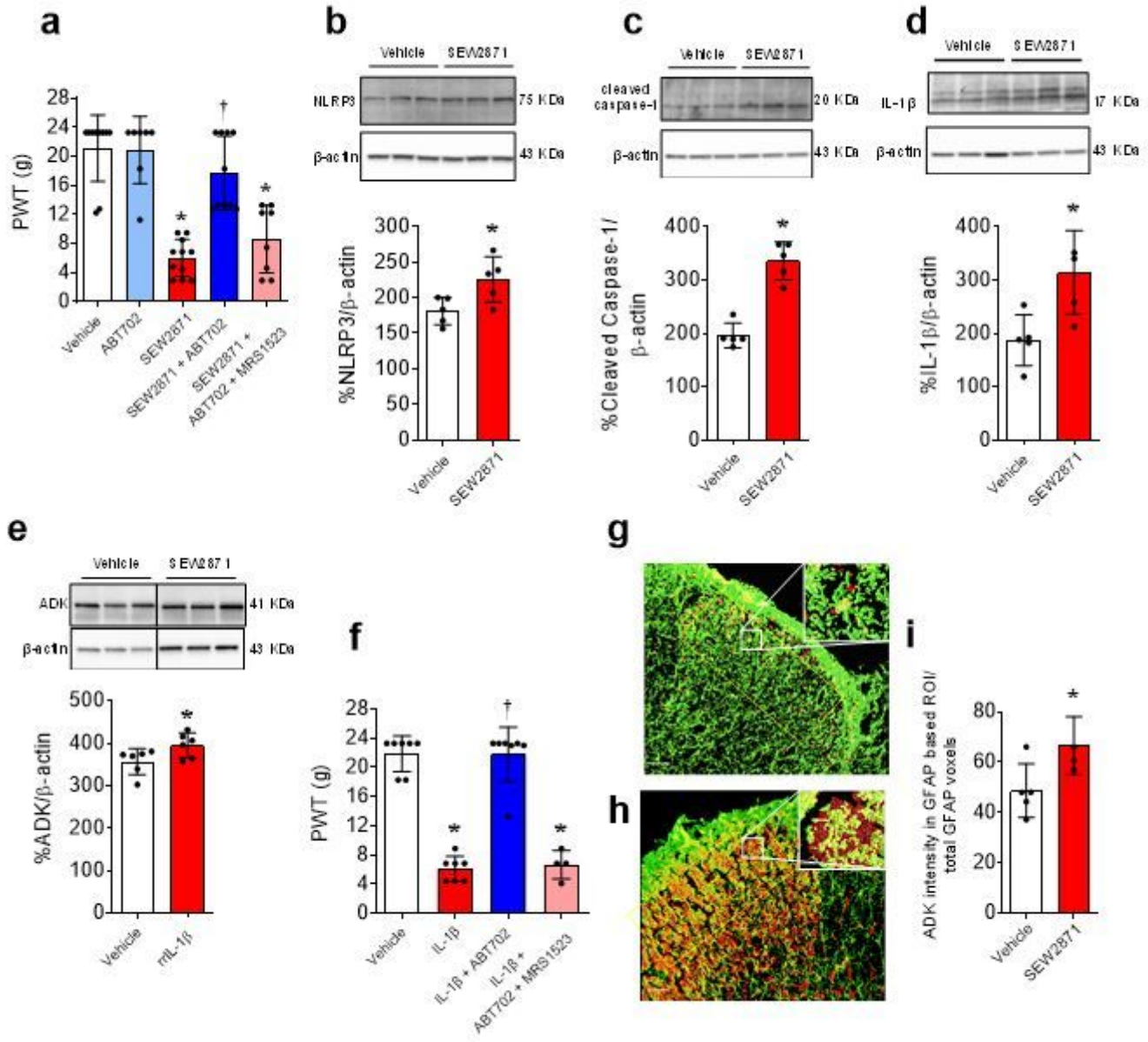

Figure 1

ADK signaling in the dorsal horn of the spinal cord drives S1PR1-induced mechano-allodynia When compared to its vehicle (3% DMSO in saline; n=6 males and n=4 females), i.th. administration of SEW2871 (2 nmol; n=6 males and n=4 females) induces mechano-allodynia in both male and female rats with peak effects reached at 2 hours after injection (a). The development of mechano-allodynia was prevented by i.th. administration of the ADK inhibitor ABT702 (30 nmol; n=6 males and n=4 females). I.th. injection of the A3AR antagonist MRS1523 (3 nmol; n=4 males and n=4 females) blocked the beneficial effect induced by ABT702 (30 nmol) (a). Levels of NLRP3 (b, n=5), cleaved caspase-1 (c, n=5) and IL-1β (d, n=5) in DH-SC harvested from SEW2871-treated rats were significantly increased when compared to DH-SC harvested from rats 2 h after i.th. vehicle (b-c-d, n=5). Results are expressed as mean ± SD for n rats and analyzed by one-way ANOVA with Tukey's comparisons (a, f) or student's t test (b-e). *p < 0.05 vs vehicle, † p < 0.05 vs SEW2871 (a-f). ADK protein expression (e, n=6) in DH-SC harvested from rrIL-1β-

treated rats were significantly increased when compared to DH-SC harvested from rats 1 h after i.th. vehicle (e, n=6). Results are expressed as mean ± SD for n rats and analyzed by one-way ANOVA with student's t test (e). When compared with its vehicle (3% DMSO in saline; n=7), i.th. administration of rrIL-1β (100 ng; n =7) induced mechano-allodynia with peak effects reached at 1 hour after injection (f). The development of mechano-allodynia was prevented by i.th. administration of the adenosine kinase inhibitor ABT702 (30 nmol; n= 7). I.th. injection of A3AR antagonist MRS1523 (3 nmol; n=4) blocked the beneficial effect induced by ABT702 (30 nmol) (f). Results are expressed as mean ± SD for n rats and analyzed by one-way ANOVA with Tukey's comparisons (f). *p < 0.05 vs vehicle, † p < 0.05 vs IL-1β. Representative images of the dorsal horn from immunofluorescence studies show increased ADK (red) expression in animals receiving intrathecal injection of SEW2871 (2 nmol; n=4) (h) compared to vehicle (3% DMSO in saline; n=5)-treated animals (g). This increase is particularly prominent among astrocytes (GFAP, green) (see inset in panels) from lamina I and II (approximately bounded by yellow box). The ADK signal associated with astrocytes is significantly increased in SEW2871-treated animals compared to vehicle-treated animals (i). Results are expressed as mean ± SD for n rats and analyzed by student's t test (i). *p < 0.5 vs vehicle.

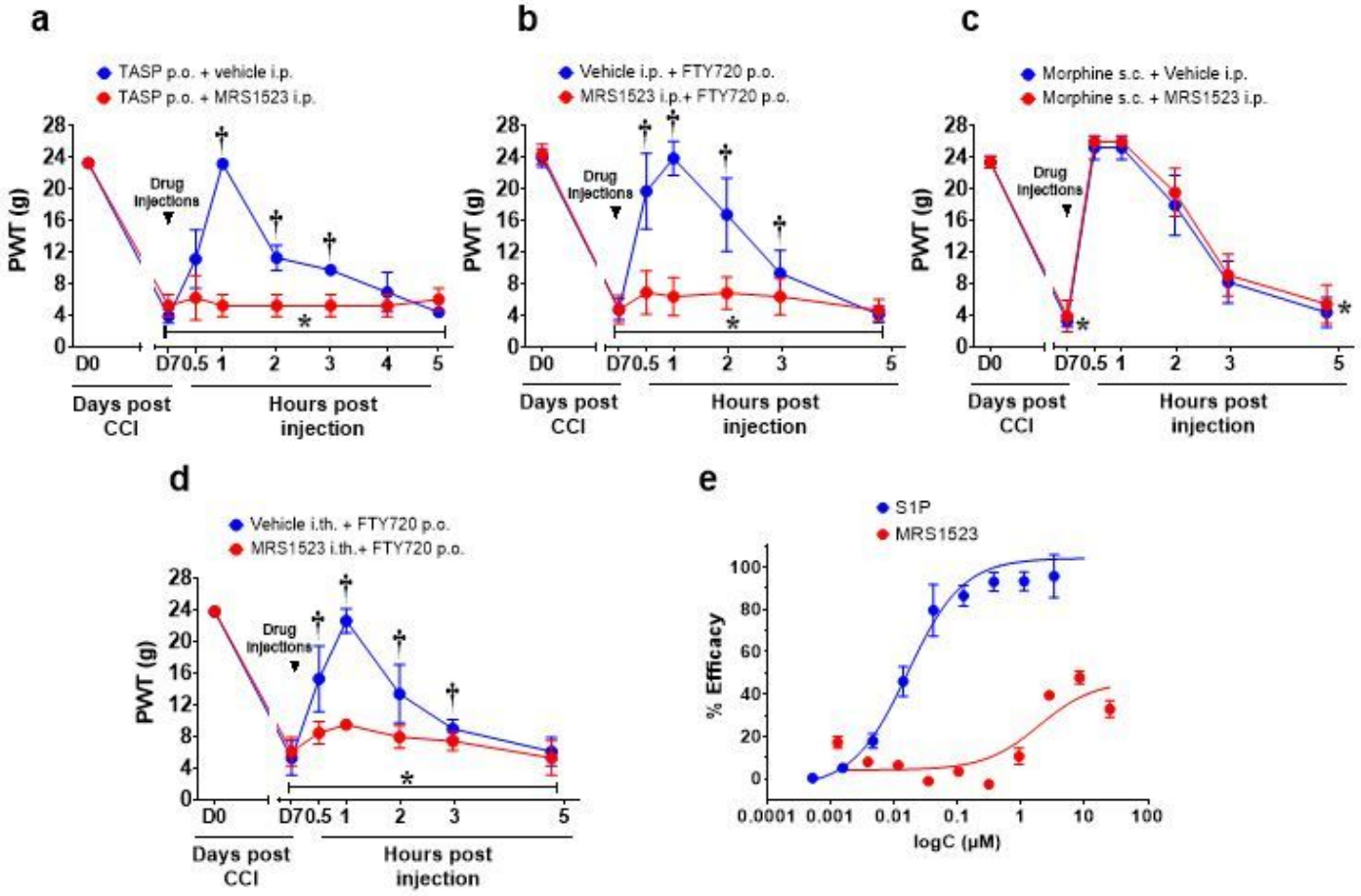

Figure 2

Deficits in adenosine signaling at the A3AR contribute to the pronociceptive actions of S1PR1 activation In rats with established neuropathic pain, mechano-allodynia was reversed by an acute oral administration on day 7 post-CCI of selective S1PR1 antagonists TASP0277308 (a, 3 mg/kg; n=3) and FTY720 (b, 3 mg/kg; n=6). An i.p. injection of the A3AR antagonist MSR1523 (5 μmol/kg) blocked the anti-allodynic effects of TASP0277308 (a, n=3) and FTY720 (b, n=6). The anti-allodynic effects of morphine were not affected by MRS1523 (c, 3 mg/kg; n=4). Furthermore, i.th. injection of MRS1523 (3 nmol; n=5) blocked the anti-allodynic effects of FTY720 given systemically (orally) (d, n=5). Results are expressed as mean ± SD for n animals and analyzed by two-way repeated measures ANOVA with Dunnett's comparisons. *$p < 0.05$ vs day 0 and † $P<0.05$ versus day 7 = (a-d). MRS1523 tested in antagonist mode with the The PathHunter® β-Arrestin assay vs control dose response curve (S1P) for the selected GPCR Biosensor Assay (e). Data represent two point determinations at each concentration tested (e).

Supplementary Files

This is a list of supplementary files associated with this preprint. Click to download.

- Supplementalmaterials.docx